Eur. Phys. J. B **31**, 391–400 (2003)
DOI: 10.1140/epjb/e2003-00047-1

THE EUROPEAN PHYSICAL JOURNAL B

Dynamic magnetization of γ-Fe_2O_3 nanoparticles isolated in an SiO_2 amorphous matrix

C. Caizer[a] and I. Hrianca

Department of Electricity and Magnetism, Faculty of Physics, West University of Timisoara, Bd. V. Parvan no. 4, 1900 Timisoara, Romania

Received 25 April 2002 / Received in final form 11 August 2002
Published online 14 February 2003 –

Abstract. We have studied the magnetization of a system of γ-Fe_2O_3 (0.68 vol.%) nanoparticles isolated in an SiO_2 amorphous matrix placed in an alternating magnetic field with a frequency of 640 Hz and in the temperature range of (77–300) K. Compared to temperatures closer to 300 K (where the system has a superparamagnetic behaviour), at lower temperatures, the magnetization has a dynamic hysteresis loop due to the magnetization's phase shift between the field and the magnetization. The delay of the magnetization (attributed to the Néel relaxation processes) increases with the decrease of temperature. It has been shown that the relaxation time resulting from the Néel theory is determined by an effective anisotropy constant (K_{eff}) that takes into account the magnetocrystalline anisotropy, as well as the shape, surface and strain anisotropies. In the following we will show that the surface and strain anisotropy components have the most significant influence. When the temperature decreases from 300 to 77 K, the relative increase of the saturation magnetization of the nanoparticles is much higher than that of the (spontaneous) saturation magnetization of bulk γ-Fe_2O_3. This increase is due to the increase of the mean magnetic diameter of the particles attached to the core of aligned spins, from 10.16 nm to 11.70 nm, as a result of the modification of the superexchange interaction in the surface layer.

PACS. 75.50.Gg Ferrimagnetics – 75.50.Tt Fine-particle systems; nanocrystalline materials – 75.60.Ej Magnetization curves, hysteresis, Barkhausen and related effects

1 Introduction

The magnetic properties of nanoparticles dispersed in different media (liquid or solid) differ significantly from those of the bulk material [1–7]. They depend to a great extent on the surface/volume ratio of the nanoparticles. When this ratio is high, the surface effect may predominate. Due to their properties, nanoparticles have found various applications *e.g.* in obtaining advanced materials for data recording and storage, medical imaging, chemistry and biology [8–10]. The nanoparticles can be prepared through physical or chemical methods. The most important aspects that influence the properties of nanoparticles and which we have to keep in mind when preparing the nanoparticles are the following: obtaining a distribution as homogenous as possible, and isolating and controlling the dimension of the nanoparticles. One of the methods that meet these requirements under certain conditions is the sol-gel method. With this method, we have obtained γ-Fe_2O_3 nanoparticles dispersed in organic polymers [11,12] or in a silica matrix [13–19]. The sol-gel method is a suitable method for sequestering the Fe ions inside the nanopores of the silica matrix. The porous matrix is made up of polysiloxane that was obtained by hydrolysis and condensation of alkoxysilane precursors. The clusters of iron ions are formed *in situ* and, after thermal treatment, they crystallize in nanopores of the iron oxide phase, and are then defined as well-isolated nanoparticles.

In the case of thermodynamic equilibrium, in the absence of interactions between the particles, the magnetic behaviour of these systems is superparamagnetic (SPM) [20,21] and similar to ferrofluids. The evolution of the magnetization M as a function of the field H follows a Langevin-type law [22]

$$M/M_\infty = L(\zeta) = \coth\zeta - 1/\zeta, \tag{1}$$

where

$$\zeta = \beta H/T = \mu_0 m_p H/k_B T. \tag{2}$$

M_∞ is the saturation magnetization of the system (magnetization in an infinite field), m_p is the magnetic moment of the particle, T is the temperature, k_B is Boltzmann's constant, and μ_0 is the vacuum magnetic permeability. Unlike ferrofluids, the magnetization axes of the magnetic nanoparticles dispersed in a solid matrix are fixed because the Brownian movement is blocked. As a result, considering the two possible relaxation mechanisms (Néel and

[a] e-mail: ccaizer@physics.uvt.ro

Brown), only the Néel-type relaxation can take place. The corresponding relaxation time is [23,24]

$$\tau_N = \tau_0 \exp(KV/k_BT), \tag{3}$$

where K is the magneto-crystalline anisotropy constant and V is the volume of the particle. τ_0 is a time constant and usually has a value of $\tau_0 \cong 10^{-9}$ s.

Most research concerning the magnetic behaviour of γ-Fe_2O_3 nanoparticles dispersed in a solid matrix was made under static conditions with SQUID (superconducting quantum interference device) [14,16,25,26] or VSM (vibrating sample) [15,27,28] magnetometers, where the measuring time was of the order of 10 to 100 s. Under dynamic conditions (at different frequencies), all studies have focussed on magnetic susceptibility [29–32]. There are no systematic studies on the dynamic magnetization or magnetic relaxation processes in high fields. Under dynamic conditions, if the frequency of the alternating field is sufficiently high, the *thermodynamic equilibrium* states of the magnetization do not have sufficient time to arise due to the relaxation processes. Consequently, the system evolves under conditions of *thermodynamic non-equilibrium*. The magnetization phase will be delayed compared to the field and the dependence M-H forms a dynamic hysteresis loop.

In this paper, we have studied the magnetization (in high fields) of γ-Fe_2O_3 nanoparticles isolated in a SiO_2 amorphous matrix, with a magnetic field frequency of 640 Hz, *i.e.* the evolution from *equilibrium processes* to thermodynamic *non-equilibrium processes*. We achieved this evolution by modifying the relaxation time with the decrease of temperature from room temperature to the temperature of liquid nitrogen. This way, the measuring time is forced to draw closer to the value of the relaxation time. In the interpretation of the results, we have analysed the influence of various forms of anisotropy that play a decisive role in the magnetic relaxation processes.

2 Experimental

2.1 Experimental technique

The crystalline phases obtained in the nanocomposites were identified by X-ray diffraction (XRD), in a Dron 2.0 diffractometer using CuK_α radiation, at the rate of 1°/min.

The magnetic measurements were made in an alternating magnetic field with a frequency of $\nu = 640$ Hz, in the temperature range of $(77 - 300)$ K. The experimental installation is based on the fluxmeter method [33] and is shown schematically in Figure 1. The selective magnetization circuit C-L-L_c-R_H (C – tuning capacitor) tuned to the fundamental oscillation frequency (640 Hz) is supplied from the power generator (G). The sample (P) with a cylindrical shape (length 4.5 cm, diameter 4.5 mm) was inserted into the probe coil S inside the magnetization coil L, which is coaxial with the sample. The sample was placed in a teflon crucible that can be fed with liquid nitrogen. The compensation of the $\mu_0\mathbf{H}_e$ component of the magnetic induction $\mathbf{B}$ ($\mathbf{B} = \mu_0\mathbf{H}_e + \mu_0\mathbf{M}$) was performed with the (L_c–S_c) coil system and the input electronic circuits of the electronic block (C.E). After being processed in the C.E, the voltage signal that is proportional to the sample's magnetization together with the signal that is proportional to the H_e field (taken over from the precision resistor R_H) was applied to the data acquisition system (DAQ) connected to a computer (PC). The signal inputs and outputs were separated by the voltage followers (F). The experimental installation was calibrated by using Ni and Fe gauges. The relative deviation at the measurement of the magnetization is of only 0.15%. During a measurement the magnetic field relative variation is less than 0.24%. The demagnetising field determined by the sample's geometry $\mathbf{H}_d = -N_d\mathbf{M}$ (N_d – demagnetizing factor) is corrected by a calculation program, so the magnetization will be recorded as a function of the sample's H field ($H = H_e - H_d$). The temperature was measured with a commercial Cu-(Cu/Ni) thermocouple.

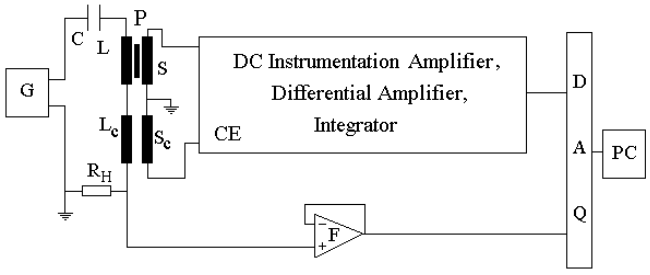

Fig. 1. Diagram of the experimental installation.

2.2 Experimental results

The nanoparticles were obtained *via* the sol-gel method based on the hydrolysis and condensation of alkoxysilane precursors, followed by heat treatment, according to the technique described in reference [34]. This procedure is similar to the procedures that have been employed by other authors [16,35]. This method can be used to obtain the ferrimagnetic phase of γ-Fe_2O_3 *in situ* at high temperatures (700–900) °C, as well as a homogeneous distribution of nanoparticles within the silica, even in the case of higher concentrations of Fe_2O_3 in SiO_2 (28.5 wt% Fe_2O_3) [16]. The nanopores formed in the matrix are the place where the iron oxide particles are nucleated, thus avoiding their aggregation [15]. The synthesis and characterization of samples obtained similarly with the sol-gel method, with different concentrations of Fe_2O_3/(Fe_2O_3-SiO_2) and treatment temperatures, were the subject of another study [34].

In this study, we focus on the dynamic magnetisation in high fields (640 Hz) of a diluted sample (where only the γ-Fe_2O_3 ferrimagnetic phase is present in the silica matrix) with a particle volume fraction of 0.68% (as shown below) and were the measuring time approaches the value of the relaxation time. Since the packing fraction is very low, the interactions between the particles are negligible [36,37]. The γ-Fe_2O_3 ferrimagnetic phase that

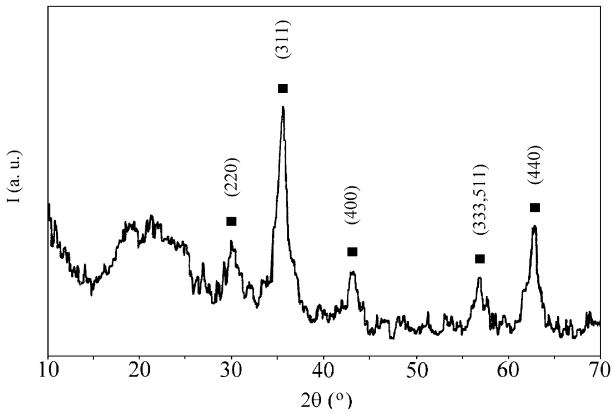

Fig. 2. X-ray diffraction pattern of the sample; ■ – γ-Fe_2O_3.

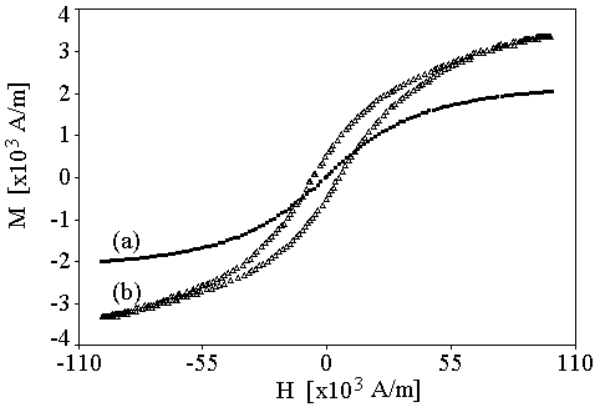

Fig. 3. Magnetization as a function of the field at the temperatures: (a) 300 K, (b) 77 K.

appears in the silica matrix after the thermal treatment of the gel at 800 °C for 3 hours was determined by X-ray diffraction (Fig. 2). The long treatment period stabilizes the γ-Fe_2O_3 phase. The XRD pattern shows that the γ-Fe_2O_3 phase is well crystallized and that the SiO_2 matrix is in an amorphous state. Our previous studies that employed infrared spectroscopy (FT-IR), XRD and Mössbauer spectroscopy [34] did not show characteristic peaks of Fe-O-Si compounds (iron silicates) that might be formed as a result of the interaction between the iron oxide and the matrix. They do in fact appear at significantly higher concentrations and treatment temperature (*e.g.* 25% wt Fe_2O_3/(Fe_2O_3-SiO_2) and 1000 °C) as in the case of the sample that was studied in this paper. At temperatures higher than 900 °C, the γ-Fe_2O_3 antiferromagnetic phase also appears. Other authors have also reported the existence of the γ-Fe_2O_3 phase at high temperatures [16,18,19,38].

The magnetization curves recorded at room temperature and the temperature of liquid nitrogen are presented in Figure 3. At 300 K, the curve has no hysteresis, while at 77 K the hysteresis loop is well outlined. Measurements made at a frequency of 50 Hz have shown that, at room temperature, there is no hysteresis (same as at 640 Hz) and at 77 K it is hardly noticeable. Increasing the temperature from 77 to 300 K, the saturation magnetization and the remanent magnetization decrease as shown in Figures 4 and 5, respectively. The AC-susceptibility (χ_{AC}) measured in the absence of the continuous magnetic field at a frequency of $\nu = 640$ Hz and an amplitude of the alternate magnetic field (H_A) of 10 Oe reaches a maximum at the temperature $T_{max} \cong 140$ K (Fig. 6).

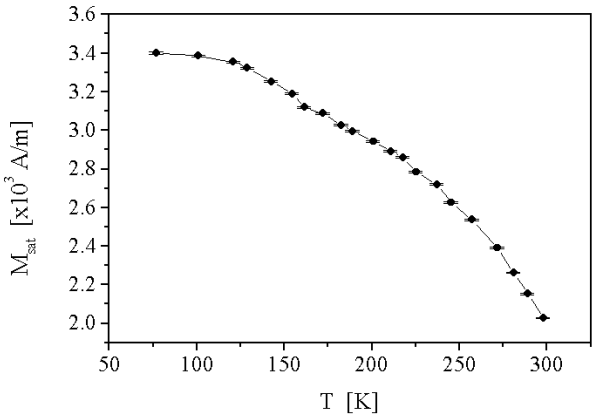

Fig. 4. Saturation magnetization M_{sat} as a function of temperature.

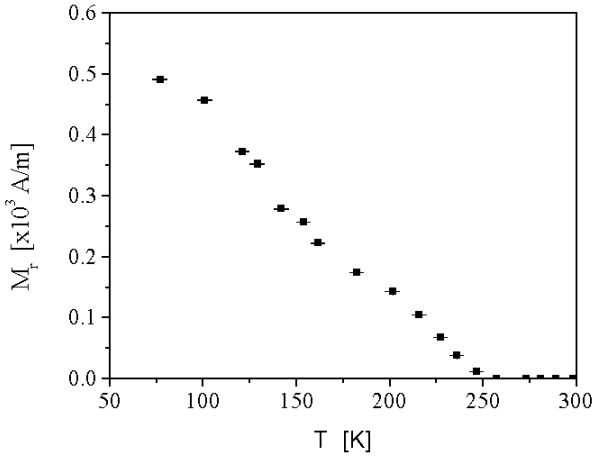

Fig. 5. Remanent magnetization M_r as a function of temperature.

3 Interpretation and discussions

3.1 Superparamagnetic behavior

Fitting the experimental values of the magnetization recorded at 640 Hz with a Langevin-type function (1), both at room temperature and at 270 K, it can be noticed that they are well aligned with the corresponding theoretical curves (Fig. 7). This result is a first argument that proves that the nanoparticle system has a superparamagnetic behaviour. However, the parameter β (Eq. (2)) – determined from the fitting – has different values for the two curves, *i.e.* $\beta_{300} = 0.0184$ m K/A at 300 K and $\beta_{270} = 0.0205$ m K/A at 270 K. For this reason, the reduced curves (Fig. 8) corresponding to the two temperatures do not overlap. Knowing that the magnetic moment

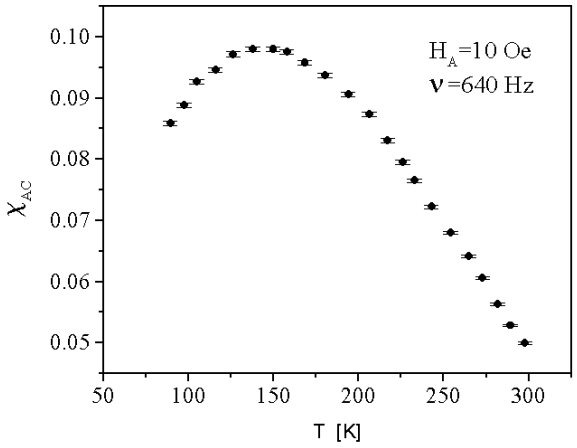

Fig. 6. Magnetic susceptibility χ_{AC} as a function of temperature.

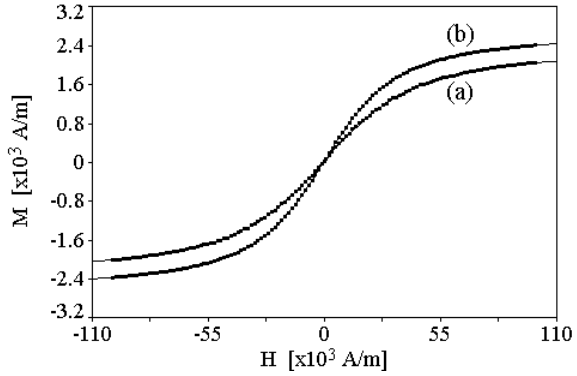

Fig. 7. Magnetization as a function of the field at the temperatures: (a) 300 K, (b) 270 K. The solid curves represent the Langevin function corresponding to the two temperatures.

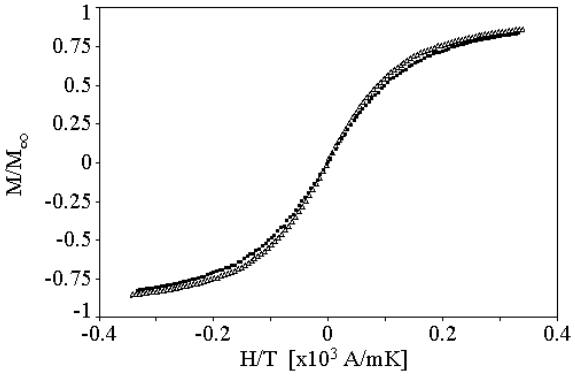

Fig. 8. Reduced magnetization M/M_∞ (M_∞ – magnetization in infinite field) as a function of H/T for the temperatures: 300 K (■) and 270 K (△).

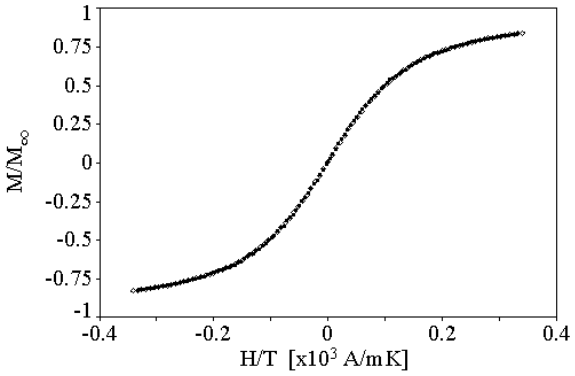

Fig. 9. Reduced magnetization as a function of H/T for the temperatures: 300 K (■) and 270 K (◇) when $\beta = \beta'_{270} = \beta_{270}/1.114$.

of the particle is $m_p = M_s V_m$ (M_s – spontaneous magnetization, V_m – magnetic volume), and taking into account the values of β that were obtained from the fit, in agreement with equation (2) we have obtained the following result:

$$\beta_{270}/\beta_{300} = (D_{m270}/D_{m300})^3 = 1.114, \qquad (4)$$

(in the approximation of spherical particles), where D_{m270} and D_{m300} are the magnetic diameters of the particles at the temperatures of 270 K and 300 K, respectively. In the temperature range (270−300) K, the spontaneous magnetization has only a slight change. Since $\beta_{270} > \beta_{300}$, we have to consider that the magnetic diameter D_m (attached to the ferrimagnetically aligned core spins) of the particles increases with the decrease of temperature. If β_{270} is replaced with $\beta_{270} = \beta_{300}$, the reduced curve corresponding to the temperature of 270 K overlaps the curve at 300 K, as shown in Figure 9. This proves that the reduced magnetization is described by a Langevin-type function and that the system has a superparamagnetic behaviour. This behaviour is also justified by the low value of the magnetic packing fraction $\varepsilon_m = M_\infty/M_s = 0.0068$, considering that at room temperature $M_\infty = 2.37 \times 10^3$ A/m (as shown later on) and $M_s = 350 \times 10^3$ A/m [39]. The low value of the packing fraction shows that the distance between the particles is relatively big so that the magnetic interactions between them can be neglected.

3.2 Mean magnetic diameter

Given that the reduced magnetization of the sample at 300 K follows a Langevin-type law, we can determine the mean magnetic diameter of the nanoparticles. In order to achieve this, we have used the values of the magnetization from the experimental curve (a) in Figure 3 both in low and high fields. Considering the fact that the particles have different diameters D_m, a more precise relation describing the magnetization is [40,41]

$$M(H,T,D_m) = n\int_0^\infty m_p(D_m)\, L[\zeta(H,T,D_m)]\, f(D_m)\, \mathrm{d}D_m, \qquad (5)$$

where n is the concentration of particles, and $f(D_m)$ is the distribution function of the diameters. In the case of the nanoparticle system, a lognormal function is well suited to describe the distribution of the particles according to their sizes – as suggested by O'Grady and Bradbury [42]

and verified experimentally by other authors [43,44]. Assuming that in our case the diameters are distributed according to the same function, $f(D_m)$ will have the expression [45]:

$$f(D_m) = \left(1/\sqrt{2\pi}\lambda_m D_m\right) \times \exp\left[-(\ln D_m - \ln D_{0m})^2/2\lambda_m^2\right], \quad (6)$$

where D_{0m} and λ_m are parameters. The mean magnetic diameter can be determined with the following equation

$$\langle D_m\rangle = D_{0m}\exp(\lambda_m^2/2), \quad (7)$$

where the distribution parameters D_{0m} and λ_m have the following expressions:

$$D_{0m} = \left[(6k_BT/\pi\mu_0 M_s H_0)\,(M_\infty/3\chi_i H_0)^{1/2}\right]^{1/3}, \quad (8)$$

$$\lambda_m = (1/3)[\ln(3\chi_i H_0/M_\infty)]^{1/2}. \quad (9)$$

Equations (8, 9) were obtained by solving the integral in equation (5) and using the approximation in low and high fields when the Langevin function becomes $L(\zeta) \to (1/3)\zeta$ and $L(\zeta) \to 1 - 1/\zeta$, respectively. The initial susceptibility $\chi_i = 0.05 \pm 2 \times 10^{-4}$ is obtained from the slope in the origin of curve $(M-H)$. $H_0 = (16.67 \pm 4 \times 10^{-2}) \times 10^3$ A/m and $M_\infty = (2.37 \pm 3.6 \times 10^{-3}) \times 10^3$ A/m result from the extrapolation of the linear part of the curve $M-1/H$. At room temperature (300 K), $\lambda_m = 0.077 \pm 2.8 \times 10^{-3}$ nm and $D_{0m} = 10.13 \pm 7.5 \times 10^{-2}$ nm. The value of the mean magnetic diameter $\langle D_m\rangle_{300} = 10.16 \pm 7.7 \times 10^{-2}$ nm and was obtained from the values determined from equation (7).

3.3 Saturation magnetization

As can be seen in Figure 4, the saturation magnetization of the sample significantly increases at the temperature of liquid nitrogen. Its relative variation in the temperature range (77–300) K is $\Delta M_{sat}/M_{sat300} = 69.7\%$ ($\Delta M_{sat} = M_{sat77} - M_{sat300}$, the subscripts representing the value of the temperature), and it is much higher than that of bulk γ-Fe_2O_3 ($\Delta M_s/M_{s300} = 9.5\%$ [10,46]) in the same temperature range. A relative increase of the saturation magnetization by $\sim 50\%$ was also observed for Fe_3O_4 nanoparticles surfacted with oleic acid and dispersed in kerosene [47]. The disorder of the spins (Fe^{3+} magnetic ions) on the surface layer of the nanoparticles is responsible for this behaviour. The constant modification of β_{270} in relation to β_{300} makes us admit that there is an increase in the mean magnetic diameter of the nanoparticles that is associated with the ferrimagnetically ordered core due to the superexchange interaction and a narrowing of the non-magnetic surface layer (where the spins are not aligned). If we take into account the value of $\langle D_m\rangle_{300}$ that was determined from equation (4), as a first approximation it results that $\langle D_{m270}\rangle = 10.53 \pm 0.08$ nm. The increase of the particles' magnetic diameter $\langle D_m\rangle$ and their magnetic moment $\langle m_p\rangle$ with the decrease of temperature has

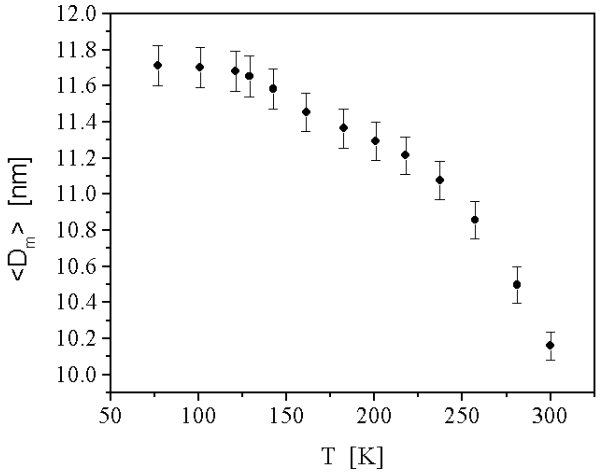

Fig. 10. Mean magnetic diameter of the particle $\langle D_m\rangle$ as a function of temperature.

to be followed by an increase of the saturation magnetization M_{sat} of the nanoparticle system. The experimental results shown in Figure 4 confirm this requirement.

The saturation magnetization can be written as follows:

$$M_{sat} = n\langle m_p\rangle = n\pi\langle D_m\rangle^3 M_s/6. \quad (10)$$

If we apply successively equation (10) for the temperatures 270 K and 300 K, respectively, the mean magnetic diameter $\langle D_m\rangle_{270}$ will have the following expression at a temperature of 270 K:

$$\langle D_m\rangle_{270} = \langle D_m\rangle_{300} \times \{[(M_{sat})_{270}(M_s)_{300}]/[(M_{sat})_{300}(M_s)_{270}]\}^{1/3}. \quad (11)$$

From the experimental data (Fig. 4) it results that $(M_{sat})_{270}/(M_{sat})_{300} = 1.18$. Taking into account that at these temperatures $(M_s)_{300}/(M_s)_{270} = 0.98$ [10,46], from equation (11) we obtain that $\langle D_m\rangle_{270} = 10.7 \pm 0.10$ nm, a result that is in good agreement with the value found from the modification of the parameter β (the relative deviation of the two values of the diameters is of only 1.6%). This fact confirms our hypothesis that the magnetic diameter attached to the core of the particle with aligned spins due to the superexchange interaction increases with the decrease of temperature. The mean magnetic diameter at other temperatures can be obtained in the same way (Fig. 10). At 77 K, it results that $\langle D_m\rangle_{77} = 11.7 \pm 0.11$ nm, which corresponds to a narrowing of the mean thickness of $\langle\delta\rangle_{77} = 0.77 \pm 0.09$ nm of the non-magnetic (paramagnetic) surface layer of the particles.

It has to be noted that, in equation (1), M_∞ corresponds to the magnetization when the magnetic moments of all particles are aligned in the same direction as the field: $M_\infty = nm_p$ This applies when the external field $H \to \infty$. If the measured values $(M_{sat})_{300}$ and $(M_{sat})_{270}$ are replaced in equation (11) with the values $(M_\infty)_{300} = 2.37 \times 10^3$ A/m and $(M_\infty)_{270} = 2.75 \times 10^3$ A/m, respectively, which were calculated in

a field of 10^8 A/m (10^3 times higher than the one used in our experiment) with equation (1), the following result is obtained: $\langle D_m\rangle'_{270} = 10.6$ nm. In fields higher than 10^8 A/m the magnetization is practically invariable. This value differs by only 0.9% from the value that was previously calculated by using the experimental values of the saturation magnetization $(M_{sat})_{300}$ and $(M_{sat})_{270}$. Furthermore, at 77 K, for the $H > 55$ kA/m the condition $\zeta = \mu_0 m_p H/k_B T \gg 1$ is met and thus the manetization in the saturation area of the nanoparticle system can be fitted with the function

$$M(H,77) = \int_0^\infty (M_\infty)_{77}(1-1/\zeta)f(D_m)\mathrm{d}D_m = (M_\infty)_{77}(1-a/H) \quad (12)$$

where

$$a = 6k_B T \exp\left(9\lambda_m^2/2\right) / \left(\pi\mu_0 M_s D_{0m}^3\right). \quad (13)$$

The best fit – considering a and $(M_\infty)_{77}$ as parameters – was obtained for $(M_\infty)_{77} = 4.20$ kA/m. If we now replace in equation (11) the ratio $(M_{sat})_{77}/(M_{sat})_{300}$ with the ratio $(M_\infty)_{77}/(M_\infty)_{300}$ we obtain the value of the magnetic diameter at 77 K, $\langle D_m\rangle'_{77} = 11.9$ nm. The relative error for the value of the diameter at 77 K, considering the magnetization $(M_{sat})_{77}$ in a field of 10^5 A/m, as compared to the case when the magnetization $(M_\infty)_{77}$ was considered in a field of 10^8 A/m, is of only 1.7%. This way, since the difference $\Delta M = M_\infty - M_{sat}$ is small (*e.g.* at 300 K, $\Delta M/M_\infty$ is 14.8%) and it always has the same sign ($M_\infty > M_{sat}$), the shape of the curve in Figure 4 does not change due to the fact that, for saturation, we have used the values of the magnetization that were measured in the field of 10^5 A/m and the relative deviation of the diameter at 77 K remains within acceptable limits (1.7%).

We interpret the reduction of the thickness δ of the surface layer as being a result of the modification of the superexchange interaction between the iron ions situated close to the surface of the nanoparticles. Due to the interactions of the silica matrix with the iron oxide nanoparticles, a distortion of the crystalline lattice occurs in the surface area of the particles. Consequently, the distance between the iron ions increases, which then leads to a decrease of the superexchange interaction energy W_{sch} in the surface layer. Since the spontaneous magnetization disappears at the θ_N temperature (the ferrimagnetic–paramagnetic transition temperature) where $W_{sch} \cong k_B\theta_N$ [48], it follows that in the shell of the particles, the transition temperature is lower than 300 K, such that at room temperature the shell is paramagnetic. We consider that the surface layer with a thickness δ is made up of several sub-layers with a thickness δ_n. Since the resulting distortion decreases towards the core of the particle, the energy of the superexchange interaction W_{sch} and implicitly the transition temperature increases from the minimum value θ_{Ns} (corresponding to the first paramagnetic layer from the surface), to the maximum value θ_N (corresponding to the ferrimagnetic core). As the temperature T decreases below room temperature, ($T < \theta_{N(n-1)}$ then $T < \theta_{N(n-2)}$, ...), the sub-layers $(n-1)$, $(n-2)$, ..., will be successively below their transition temperatures $\theta_{N(n-1)}$, $\theta_{N(n-2)}$, ... Consequently, these sub-layers will become ferrimagnetically ordered. This ordering starts in the first sub-layer of the particle next to the magnetic core and progresses towards the surface as the temperature decreases. Thus, with the decrease of temperature the diameter of the magnetic core increases to the detriment of the paramagnetic layer, which is progressively thinner. Hence, the magnetic moment of the particles $m_p(D_m,T) = \pi M_s(T)D_m(T)^3/6$ increases and this leads to the large increase of the saturation magnetization of the nanoparticle system

$$M_{sat}(D_m,T) = n\int_{(T)} \left(\frac{\left(\int_0^\infty m_p(D_m,T)f(D_m)\mathrm{d}D_m\right)}{\left(\int_0^\infty f(D_m)\mathrm{d}D_m\right)}\right)\mathrm{d}T \quad (14)$$

with the decrease of temperature. In equation (14)

$$\frac{\left(\int_0^\infty m_p(D_m,T)f(D_m)\mathrm{d}D_m\right)}{\left(\int_0^\infty f(D_m)\mathrm{d}D_m\right)} = \langle m_p(D_m,T)\rangle \quad (15)$$

is the mean of the magnetic moments of the particles at a temperature T.

The existence of surface spin disorder has been proven experimentally. Thus, for the γ-Fe_2O_3 nanoparticles isolated in a silica matrix, obtained by the sol-gel method and calcination of the gel at high temperatures (700−900) °C, two absorption lines $g \sim 2$ and $g \sim 4.3$ [16] were observed using electron spin resonance (ESR). The first line, according to Sharma and Waldner [49], is due to the ferrimagnetic resonance of the single domain particles that are randomly oriented, since the temperature dependence of the lines can be explained with the Raikher and Stepanov model [50]. The second line has been attributed to a strong disordered spin state at the surface of the particles. At the same time, it has been shown that the mean physical diameter of the nanoparticles resulting from transmission electron microscopy (TEM) is higher than the mean magnetic diameter that resulted from magnetic measurements [16]. By means of Mossbauer spectroscopy at room temperature [18] it has been shown that, after fitting, the experimental data correspond to two states: an ordered state, attributed to the Fe^{3+} ions inside the particle and a disordered state, attributed to the ions in the surface layer of the particle. Tronc *et al.* [51] have obtained similar results by means of Mossbauer spectroscopy for the γ-Fe_2O_3 phosphated nanoparticles (with a diameter of 4.6 nm). The authors have shown that the surface layer of the nanoparticles is paramagnetic until a temperature of ca. 20 K is reached. These results confirm the existence of the surface layer of the particles, where the Fe^{3+} magnetic ions are in a disordered (paramagnetic) structure; the thickness of the surface layer has an order of magnitude of 10^{-1} nm.

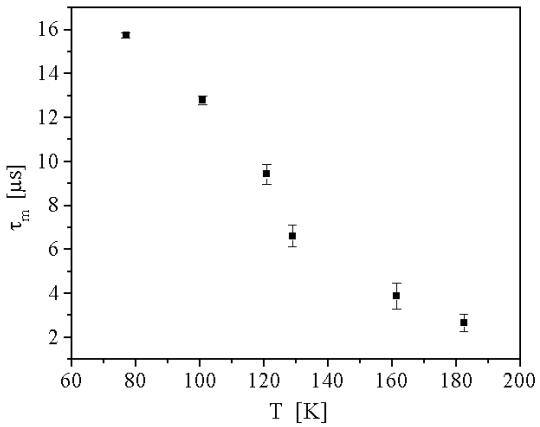

Fig. 11. Delay time τ_m as a function of temperature.

3.4 Relaxation time. Dynamic hysteresis loop

By representing the values of M and H that were determined experimentally as a function of time, we have observed that at low temperatures they do not pass simultaneously through the zero value; namely the magnetization is delayed compared to the magnetic field. The experimental results show that the delay time τ_m increases with the decrease of temperature (Fig. 11). This implies a phase shift of the magnetization by $\varphi_m = \omega\tau_m$ (ω – angular velocity) compared to the field. For example, at 77 K the delay time was of 15.7 ± 0.11 μs and the phase shift corresponding to this time was of 0.0631 rad.

In order to check if the observed phase shift can lead to the experimentally observed dynamic hysteresis, we have determined the functions $H(t)$ and $M(t)$ corresponding to the hysteresis loop in Figure 3b

$$H(t) = H_{max}\sin(\omega t + \varphi_m);\ (\varphi_m > 0), \tag{16}$$

$$M(t) = \sum_{n=1}^{\infty} M_n \sin(n\omega t). \tag{17}$$

where $H_{max} = 100 \times 10^3$ A/m. We have calculated the Fourier coefficients M_n up to the order of $n = 75$ on the basis of the experimental values using real time Fast-Fourier transform (FFT). We have then represented the pairs of values found with the equations (16, 17) in the (M, H) plane of Figure 12 (solid curve). The fact that the calculated values are in good agreement with the experimentally measured values demonstrates that the existence of the phase shift between the two observables causes the dynamic character of the hysteresis loop. The phase shift appears as a consequence of the relaxation processes.

If the magnetic anisotropy is reduced to the magnetocrystalline component, with the known values of the magnetocrystalline anisotropy constant (K_ν), the relaxation times (τ_N) obtained with equation (3) would be of the order of magnitude 10^{-8}–10^{-9} s (*e.g.* three or four orders of magnitude smaller than the times τ_m that we have measured). This way, even at 77 K the sample should have a superparamagnetic behaviour. This difference indicates that, besides the magnetocrystalline anisotropy, the shape

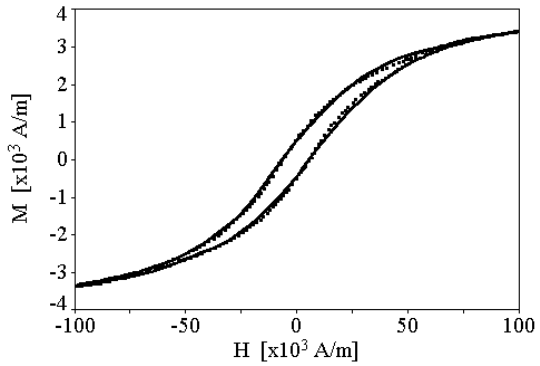

Fig. 12. Dynamic hysteresis loop determined with the equations (16, 17) at 77 K; (■) experimental values.

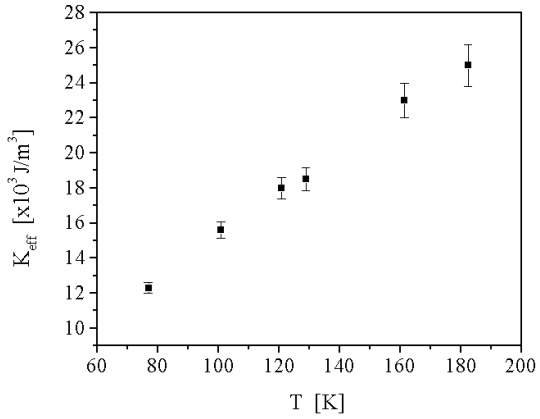

Fig. 13. Effective anisotropy constant K_{eff} as a function of temperature.

and surface anisotropies [52] have a significant influence. Since the particles are embedded in a solid matrix, the interface can exert a strain on the particles. Thus, in the equation (3), K is an effective anisotropy constant (K_{eff})

$$K_{eff} = K_\nu + K_{sh} + K_s + K_{st}, \tag{18}$$

where K_{sh} is the shape anisotropy constant, $K_s = K'_s 6/\langle D_m\rangle$ [53] where K'_s (in J/m^2) is the surface anisotropy constant and K_{st} is the strain anisotropy constant. Thus, according to equation (3), the relaxation time is

$$\tau = \tau_0 \exp(K_{eff}\langle V_m\rangle/k_B T). \tag{19}$$

If we consider that the time corresponding to the phase shift is equal to the relaxation time ($\tau_m = \tau$), from equation (19) it results that

$$K_{eff} = \left(6k_B T/\pi\langle D_m\rangle^3\right)\ln(\tau_m/\tau_0). \tag{20}$$

We have calculated K_{eff} at different temperatures (Fig. 13), using the resulting values of $\langle D_m\rangle$ (Fig. 10) and τ_m (Fig. 11). Fitting the points in the figure and extrapolating the curve ($K_{eff} - T$) at room temperature, we obtain the following value: $K_{eff} = 4 \times 10^4$ J/m^3, a value that has an order of magnitude higher than $K_\nu = 4.6 \times 10^3$ J/m^3 [54,55] corresponding to bulk γ-Fe_2O_3.

Other authors have obtained higher values of K_{eff} (up to one order of magnitude higher) for γ-Fe_2O_3 nanoparticles at room temperature, than the values we have obtained. Vassiliou *et al.* [56] obtained a value of 4.4×10^5 J/m^3 for particles with a diameter of 8.3 nm in a polymer matrix, and Coey *et al.* [57] obtained a value of 1.2×10^5 J/m^3 for particles with a diameter of 6.5 nm. These higher values can be attributed to the smaller diameter of the nanoparticles (in the case of smaller particle diameters the surface effect is more significant) and to the fact that they are dispersed in different matrices. Thus, in the case of γ-Fe_2O_3 nanoparticles with a diameter of ∼15 nm the value of the effective anisotropy constant is of 4×10^4 J/m^3 [58], a value that is in good agreement with the value that we have determined.

If we consider that the particles have the shape of rotation ellipsoids, the shape anisotropy constant can be determined with the relation

$$K_{sh} = -(1/2)(N_z - N_y)\mu_0 M_s^2, \tag{21}$$

where N_z and N_y are the demagnetising factors, considering z, y and x as being the axes of the ellipsoid ($z > y = x$). Taking into account the values of these factors [59] and considering a mean ellipticity of the particles of 1.1, we obtain $K_{sh} = 2.9 \times 10^3$ J/m^3. Taking into consideration the values determined for the K_ν and K_{sh} constants, according to equation (18) it results that the surface and the strain anisotropies have the most significant contribution to the magnetic anisotropy. However, if we assume that $K'_s \sim 10^{-5}$ J/m^3 [53] (for nanoparticles with a diameter of ∼ 10 nm at room temperature), then K_s is $\sim 6 \times 10^3$ J/m^3. According to this result we can state that at higher temperatures (closer to room temperature), the strain determines the magnetic anisotropy. With the decrease of temperature T, the K_{eff} constant decreases as shown in Figure 13. The decrease of the K_{eff} constant can be attributed both to the decrease of K_s due to the increase of the magnetic diameter of the particles (according to Néel [52] and Papusoi [53]) and to the modification of strain exerted by the interface of the silica matrix on the particles (K_{st}). Since the particles are isolated in the matrix it is difficult to separate the surface effect from the strain effect and to establish the contribution of each component to the total anisotropy. But if we take into consideration that the increase of the magnetic diameter is not very high, the decrease of the constant K_{eff} can be attributed to a large extent to the decrease of K_{st}. Due to the fact that in the temperature range that was considered for our study the average volume dilatation coefficient of the particle ($\langle\alpha_p\rangle$) is sensibly higher than the average volume dilatation coefficient of the matrix (amorphous SiO_2) ($\langle\alpha_m\rangle$), at the decrease of temperature there will be a higher decrease of the particle volume than the volume of the matrix cavities that surround the particles. Consequently, there will be a weakening of the strain exerted by the interface on the particle, which leads to a decrease of the constant K_{st} and implicitly of the constant K_{eff}.

It is known that the magnetic susceptibility has a maximum at the blocking temperature T_B when the measuring time t_m becomes equal to the relaxation time τ [60,61]. For a non-interacting particle system with a particle size distribution, the mean blocking temperature is given by T_{max}, the exact relation depending on the form of the distribution. As a first approximation, $T_{max} = \langle T_B\rangle$ for the same average volume [62,63]. In our case, the relaxation time $\tau_m = 6$ μs (Fig. 11) and the mean magnetic diameter of 11.6 nm (Fig. 10) correspond to the blocking temperature $\langle T_B\rangle = T_{max} \cong 140$ K from Figure 6. Considering that $t_m = \tau_m$ and $T = \langle T_B\rangle$, with the above-mentioned values, from equation (20) we obtain $K_{eff} = 2.0 \times 10^4$ J/m^3. This value is in very good agreement with the value corresponding to the temperature (T) of 140 K (Fig. 13) determined with other methods. This result is a further confirmation that the value of the K_{eff} constant that we have determined is correct.

Although the K_{eff} constant decreases with the decrease of temperature due to the surface effect, this decrease and the simultaneous increase of the mean magnetic diameter of the particles lead to an overall effect that results in the increase of $K_{eff}\langle V_m\rangle/k_BT$. According to equation (19), this leads to an increase of the relaxation time τ considered as being equal to the time τ_m corresponding to the phase shift (φ_m). Accordingly, the phase shift and, implicitly, the remanent magnetization, increase (Fig. 5). Under static conditions, according to the Stoner-Wolhfarth model [64] for a nanoparticle system, when the external magnetic field that saturated the sample becomes zero, the remanent magnetization will be

$$M_r = (1/2)S_B M_s. \tag{22}$$

In the case of well-isolated particles $S_B = 1$ and $M_r = M_s/2$ in the absence of thermal agitation (0 K), because the magnetic moments are randomly oriented. S_B measures the volume fraction of blocked particles at a given temperature. In our case, $S_B \sim 0.29$ at a temperature of 77 K because $M_r/M_s \sim 0.145$ (Fig. 3, curve b). This shows that at a frequency of 640 Hz of the field, approximately 30% of the particles have blocked magnetic moments and the rest (70%) may invert at 180 degrees along the easy magnetization axes due to the thermal activation. The value of 0.29 of S_B is also influenced by the increase of the frequency of the magnetization field when the measuring time (t_m) is getting closer to the relaxation time τ_m. Compared to the static case, this has the effect that a further portion of the magnetic moments, no longer being able to follow the variations of the field, are blocked at the temperature of 77 K and at a frequency of 640 Hz. When the temperature increases more and more magnetic moments receive the necessary energy to surpass the potential barrier and accordingly invert. This will lead to a gradual decrease of the remanent magnetization (Fig. 5) until it becomes zero at approximately 250 K. Above this temperature, up to 300 K, the thermodynamic equilibrium is always reached; the magnetization follows almost instantly the field and in this way the hysteresis loop disappears (Figs. 3, 5).

4 Conclusions

An examination of a system of γ-Fe_2O_3 nanoparticles isolated in a SiO_2 solid matrix and placed in a magnetic field with a frequency of 640 Hz has shown that the system has a superparamagnetic behaviour in the temperature range of (270−300) K. Below 270 K there are deviations due to the fact that a dynamic hysteresis loop appears and grows. This effect is attributed to the magnetic relaxation processes that become evident and intensify with the decrease of temperature. The determined relaxation time depends on an effective anisotropy constant K_{eff}, which is mostly influenced by the strain anisotropies. As the temperature decreases, there is a large increase in the saturation magnetization of the γ-Fe_2O_3 nanoparticles isolated in the silica matrix. In the range from 77 to 300 K the relative increase of the saturation magnetization of the nanoparticles is 7.54 times higher than that of the spontaneous magnetization of bulk ferrite. We have shown that this increase is due to the increase of the magnetic diameter of the nanoparticles where the spins are ferrimagnetically ordered.

The authors are grateful to Linde Gaz Romania for their support in obtaining low temperatures.

References

1. A.E. Berkowitz, R.H. Kodama, S.A. Makhlouf, F.T. Parker, F.E. Spada, E.J. McNiff Jr., S. Foner, J. Magn. Magn. Mater. **196-197**, 591 (1999)
2. M. El-Hilo, R.W. Chantrell, K. O'Grady, J. Appl. Phys. **84**, 5114 (1998)
3. J.L. Dormann, D. Fiorani, R. Cherkaoui, E. Tronc, F. Lucari, F. D'Orazio, L. Spinu, M. Noguès, H. Kachkachi, J.P. Jolivet, J. Magn. Magn. Mater. **203**, 23 (1999)
4. J.M.D. Coey, Phys. Rev. Lett. **27**, 1140 (1971)
5. S. Iakovenko, A. Trifonov, M. Giersig, A. Mamedov, D. Nagesha, V. Hanin, E. Soldatov, N. Kotov, Adv. Mater. **5**, 11 (1999)
6. I. Hrianca, I. Malaescu, J. Magn. Magn. Mater. **150**, 131 (1995)
7. C. Savii, M. Popovici, C. Enache, J. Subrt, D. Niznansky, S. Bakardzieva, C. Caizer, I. Hrianca, *International Symposiun on Soft Solution Processing (SSP-2000), Tokyo, 2000*, p. 72
8. J. Yong-Nam, D.M. Dabbs, I.A. Aksay, S. Erramilli, Langmuir **10**, 3377 (1994)
9. D.D. Awschalom, D.P. DiVicenzo, Phys. Today **4**, 43 (1995)
10. R.F. Ziolo, E.P. Giannelis, B.A. Weinstein, M.P. O'Horo, B.N. Ganguly, V. Mehrotra, M.W. Russell, D.R. Huffman, Science **257**, 219 (1992)
11. E. Kroll, F.M. Winnik, R.F. Ziolo, Chem. Mater. **8**, 1594 (1996)
12. G.M. da Costa, E. DeGrave, P.M.A. de Bakker, R.E. Vandenberghe, J. Solid State Chem. **113**, 405 (1994)
13. C. Chanéac, E. Tronc, J.P. Jolivet, J. Mater. Chem. **6**, 1905 (1996)
14. L. Zhang, G.C. Papaefthymiou, R.F. Ziolo, J.Y. Ying, NanoStructured Materials **9**, 185 (1997)
15. F. del Monte, M.P. Morales, D. Levy, A. Fernandez, M. Ocana, A. Roig, E. Molins, K. O'Grady, C.J. Serna, Langmuir **13**, 3627 (1997)
16. C. Cannas, D. Gatteschi, A. Musinu, G. Piccaluga, C. Sangregorio, J. Phys. Chem. B **102**, 7721 (1998)
17. M. Casu, F.C. Marincola, A. Lai, A. Musinu, G. Piccaluga, J. Non-Crystalline Solids **232-234**, 329 (1998)
18. C. Cannas, G. Concas, A. Musinu, G. Piccaluga, G. Spano, Z. Naturforsch. **54** a, 513 (1999).
19. S. Bruni, F. Cariati, M. Casu, A. Lai, A. Musinu, G. Piccaluga, S. Solinas, NanoStructured Materials **11**, 573 (1999)
20. F. Bentivegna, J. Ferré, M. Nyvlt, J.P. Jamet, D. Imhoff, M. Canva, A. Brun, P. Veillet, Š. Višňovsky, F. Chaput, J.P. Boilot, J. Apll. Phys. **83**, 7776 (1998)
21. I. Hrianca, C. Caizer, C. Savii, M. Popovoci, J. O. Adv. Matter. **2**, 634 (2000)
22. I.S. Jacobs, C.P. Bean, in *Magnetism III*, edited by G.T. Rado, H. Suhl (Academic Press, New York, 1963)
23. L. Néel, Ann. Geophys. **5**, 99 (1949)
24. A. Aharoni, Phys. Rev. A **135**, 447 (1964)
25. B. Martinez, X. Obradors, Ll. Balcells, A. Rouanet, C. Monty, Phys. Rev. Lett. **80**, 181 (1998)
26. D. Fiorani, J.L. Dormann, R. Cherkaoui, E. Tronc, F. Lucari, F. D'Orazio, L. Spinu, M. Noguès, H. Kachkachi, J.P. Jolivet, J. Magn. Magn. Mater. **203**, 23 (1999)
27. R.D. Shull, J.J. Ritter, A.J. Shapiro, L.J. Swartzendruber, L.D. Bennett, J. Appl. Phys. **67**, 4490 (1990)
28. M. Nogami, J. Mater. Sci. Lett. **12**, 1705 (1993)
29. J.L. Dormann, L. Spinu, E. Tronc, J.P. Jolivet, F. Lucari, F. D'Orazio, D. Fiorani, J. Magn. Magn. Mater. **183**, L255 (1998)
30. H. Casalta, P. Schleger, C. Bellouard, M. Hennion, I. Mirebeau, G. Ehlers, B. Farago, J.L. Dormann, M. Kelsch, M. Linde, F. Phillipp, Phys. Rev. Lett. **82**, 1301 (1999)
31. P. Svedlindh, T. Jonsson, J.L. Garcia-Palacíos, J. Magn. Magn. Mater. **169**, 323 (1997)
32. T. Jonsson, P. Nordblad, P. Svedlindh, Phys. Rev. B **57**, 497 (1998)
33. H. Zijlstra, *Experimental Methods in Magnetism* (North-Holland Publishing Company, Amsterdam, 1967)
34. C. Savii, M. Popovici, C. Enache, J. Subrt, D. Niznansky, S. Bakardzieva, C. Caizer, I. Hrianca, Solid State Ionics **151**, 219 (2002)
35. G. Concas, G. Ennas, D. Gatteschi, A. Musinu, G. Piccaluga, C. Sangregorio, G. Spano, J.L. Stanger, D. Zedda, Chem. Mater. **10**, 495 (1998)
36. P. Jönsson, T. Jonsson, J.L. Garcia-Palacíos, P. Svedlindh, J. Magn. Magn. Mater. **222**, 219 (2000)
37. L. Spinu, J.L. Dormann, M. Nogues, E. Tronc, J.P. Jolivet, J. Magn. Magn. Mater. **196-197**, 64 (1999)
38. R. Berger, J.-C. Bissey, J. Kliava, H. Daubric, C. Estournès, J. Magn. Magn. Mater. **234**, 535 (2001)
39. M.E. Schabes, H.N. Bertram, J. Appl. Phys. **67**, 5149 (1990)
40. B. Berkovsky, V. Bashtovoy, *Magnetic fluids and applications handbook* (Begell House Inc., New York, 1996)
41. A.F. Pshenichnikov, W.V. Mekhonoshin, A.V. Lebedev, J. Magn. Magn. Mater. **161**, 94 (1996)

42. K, O'Grady, A. Bradbury, J. Magn. Magn. Mater. **39**, 91 (1994)
43. I.I. Yaacob, A.C. Nunes, A. Bose, J. Colloid Interface Sci. **171**, 73 (1995)
44. N. Moumen, M.P. Pileni, Chem. Mater. **8**, 11128 (1996)
45. J.C. Bacri, R. Perzinski, D. Salin, V. Cabuil, R. Massart, J. Magn. Magn. Mater. **62**, 36 (1986)
46. A.E. Berkowitz, W.J. Schuele, P.J. Flanders, J. Appl. Phys. **39**, 1261 (1968)
47. I. Hrianca, C. Caizer, Z. Schlett, J. Appl. Phys. **92**, 2125 (2002)
48. R. Valenzuela, *Magnetic ceramics* (Cambridge University Press, Cambridge, 1994)
49. V.K. Sharma, F. Waldner, J. Appl. Phys. **48**, 4298 (1997)
50. Yu.L. Raikher, V.I. Stepanov, Phys. Rev. B **50**, 6250 (1994)
51. E. Tronc, A. Ezzir, R. Cherkaoui, C. Chanéac, M. Noguès, H. Kachkachi, D. Fiorani, A.M. Testa, J.M. Grenèche, J.P. Jolivet, J. Magn. Magn. Mater. **221**, 63 (2000)
52. L. Néel, J. Phys. Rad. **15**, 225 (1954)
53. C. Papusoi Jr., J. Magn. Magn. Mater. **195**, 708 (1999)
54. A.H. Morrish, E.P. Valstyn, J. Phys. Soc. Jpn **17**, 392 (1962)
55. S. Mørup, J. Magn. Magn. Mater. **37**, 39 (1983)
56. J.K. Vassiliou, V. Mehrotra, M.W. Russell, E.P. Giannelis, J. Appl. Phys. **73**, 5109 (1993)
57. J.M.D. Coey, D. Khalafalla, Phys. Status Solidi (a) **11**, 229 (1972)
58. B. Martinez, A. Roig, X. Obradors, E. Molins, P. Claret, C. Monty, J. Appl. Phys. **79**, 2580 (1996)
59. E. Kneller, Ferromagnetismus (Springer, Berlin, 1962)
60. L. Néel, Adv. Phys. **4**, 191 (1955)
61. J. Mira, J.A. López-Pérez, J. Rivas, M.A. López-Quintela, IEEE Trans. Magn. **33**, 3724 (1997)
62. J.L. Dormann, F. D'Orazio, F. Lucari, E. Tronc, P. Prené, J.P. Jolivet, D. Fiorani, R. Cherkaoui, M. Nogués, Phys. Rev. B **53**, 14291 (1996)
63. K. O'Grady, M. El-Hilo, R.W. Chantrell, IEEE Trans. Magn. **29**, 2608 (1993)
64. E.C. Stoner, E.P. Wohlfarth, Philos. Trans. R. Soc. London, Ser. A **240**, 599 (1948)